社団法人 情報処理学会　研究報告
IPSJ SIG Technical Report

2004－CVIM－144　(28)
2004／5／7

6 自由度カメラ運動の下での Multiperspective Imaging によるステレオ[1]

市村 直幸

産業技術総合研究所 情報処理研究部門
〒 305-8568 つくば市梅園 1-1-1 中央第二
nic@ni.aist.go.jp, http://staff.aist.go.jp/naoyuki.ichimura/

あらまし　Multiperspective Imaging によるステレオは，シーンの 3 次元構造復元のための一手法である．現在まで，ステレオパノラマを代表とする構造復元のための種々のアルゴリズムが提案されているが，ステレオ画像を取得するためのカメラ運動に制約があった．本論文では，6 自由度カメラ運動を考慮した Multiperspective Imaging によるステレオの枠組みを提案する．ステレオ画像の取得をラインカメラによってモデル化し，それに基づき構造復元に必要な幾何拘束およびエピポーラ曲線の式を導出する．その結果に基づき，提案する枠組みが，従来の Multiperspective Imaging に基づくステレオを特別な場合として包含していることを示す．導出した式に基づき，いくつかの実験例を示す．

Stereo by Multiperspective Imaging under 6 DOF Camera Motion

Naoyuki ICHIMURA

Information Technology Research Institute
National Institute of Advanced Industrial Science and Technology (AIST)
Tsukuba Central 2, 1-1-1, Umezono, Tsukuba, Ibaraki, 305-8568 Japan
nic@ni.aist.go.jp, http://staff.aist.go.jp/naoyuki.ichimura/

Abstract　Multiperspective imaging has been used to recover the structure of a scene. Although several algorithms for structure recovery have been developed as typified by stereo panoramas, there exists no common framework which subsumes various camera motions to capture stereo images. This paper presents a framework for stereo by multiperspective imaging, which is general in that it can handle 6 degree–of–freedom (DOF) camera motion. We derive geometric constraints, equation for structure recovery and that for an epipolar curve by modeling the acquisition of stereo images using pushbroom cameras (line sensors). We consider a class of camera motion called a vertical view plane class and demonstrate that several previous results are really special cases of our results. Experimental results are given to show the correctness of the equations derived.

[1]This work was supported in parts by the JSPS Overseas Research Fellowship.

1 Introduction

Multiperspective imaging which uses multiple view points to construct images has attracted attention as a method to recover structure of a scene. A typical example is stereo panoramas, where one-dimensional (1D) images, e.g., columns extracted from two-dimensional (2D) images, corresponding to different view points are concatenated to capture stereo images. Recently several investigators have used the stereo panoramas for structure recovery. An approach is to use rotating cameras. Ishiguro et al. [8] were the first to use stereo panoramas captured by a rotating camera. Peleg et al. [9] proposed the method to capture stereo panoramas using a single rotating camera. Shum et al. [10] presented the approach called concentric mosaics in which camera motion is constrained to planar concentric circles. Epipolar geometry of the concentric mosaics was considered by Huang [11]. Perr et al. [12] and Huang et al. [13] also used rotation to capture stereo panoramas. An alternative approach is to use translating cameras. Gupta et al. [14] investigated epipolar geometry between images captured by two pushbroom cameras (also known as line scanners/sensors) moving on a line. Chai et al. [15] and Zhu et al. [16] proposed stereo reconstruction based on parallel projections realized by a camera with 1D, 2D and three-dimensional (3D) translations. Feldman et. al. [17] showed the epipolar geometry of the stereo by a crossed-slits projection [18] which includes the linear pushbroom projection [14] as a special case. It is important to note that analysis for structure recovery and epipolar geometry were carried out *separately* for rotation and translation in previous work; there exists no common framework which subsumes various camera motions to capture stereo panoramas.

This paper presents a general framework for structure recovery using stereo images captured by multiperspective imaging. In the framework, we use a pushbroom camera which is an imaging system with a 1D array of pixels to model the acquisition of an image. Figure 1(a) shows a scene being scanned by a moving pushbroom camera. At each instant of time, the camera produces a 1D image which represents the brightness of the scene points that intersect the "view plane" of the camera. By concatenating consecutive 1D images, we obtain an image (panorama), such as the one in Fig. 1(b). If we have two cameras, we can compute the structure of a scene using a parallax between two acquired images.

Stereo using pushbroom cameras has been used for photogrammetry and remote sensing. Since cameras are mounted on satellites or airplanes,

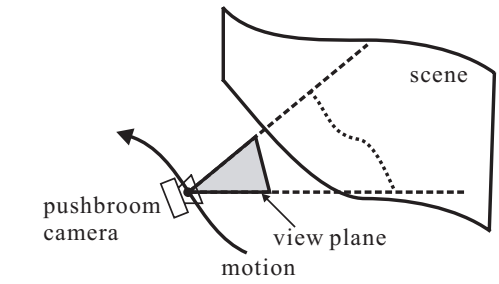

(a)

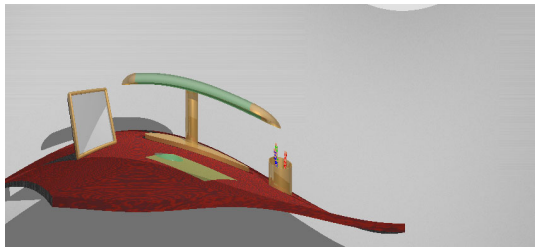

(b)

Figure 1: The acquisition of an image by a pushbroom camera. (a) A moving pushbroom camera sweeps a scene with the "view plane". A 1D image, which represents the brightness of the scene points that intersect the view plane, is produced at each instant of time. (b) An example of an image created by concatenating the 1D images.

camera motion could be complex. Simplified camera motion model with a small number of degree-of-freedom (DOF), however, can be used because of the assumptions of the large distance between the cameras and the ground and smooth motion of the cameras [14, 19, 20]. Since we cannot use the assumption of the large distance in the field of computer vision, consideration for 6 DOF motion is necessary. Recently Seitz et. al. [21] presented a framework for stereo by multiperspective imaging which includes stereo using pushbroom cameras, but camera motion was restricted because they considered "rectified" stereo pairs.

We should consider imaging geometry, structure recovery and epipolar geometry to make the framework of stereo by multiperspective imaging. First we derive geometric constraints including a *view plane equation* using the imaging geometry of a pushbroom camera. Then we show explicit representation of equation for structure recovery and that for an epipolar curve based on the constraints. The framework is general in that it can handle 6 DOF motion of the camera. We consider a class of camera motion called a vertical view plane class and demonstrate that several previous results are really special cases of our results. We conclude with examples of epipolar curves to show the correctness of the equations derived.

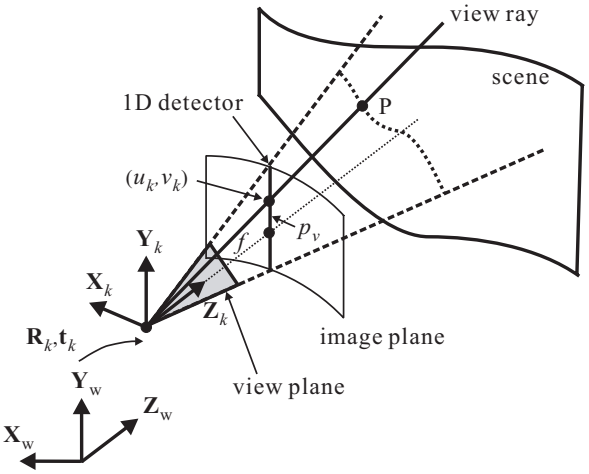

Figure 2: Imaging geometry of a pushbroom camera. The world coordinate system is denoted by the $\boldsymbol{X}_{\mathrm{w}}$, $\boldsymbol{Y}_{\mathrm{w}}$ and $\boldsymbol{Z}_{\mathrm{w}}$ axes. The camera coordinate system at the instant of time kT_s is denoted by the $\boldsymbol{X}_k$, $\boldsymbol{Y}_k$ and $\boldsymbol{Z}_k$ axes. The relationship between the world and camera coordinate systems is given by the rotation matrix $\boldsymbol{R}_k$ and translation vector $\boldsymbol{t}_k$. The world and camera coordinates of a 3D point P are $\boldsymbol{p}_w = (\mathrm{x_w}, \mathrm{y_w}, \mathrm{z_w})^t$ and $\boldsymbol{p}_k = (\mathrm{x}_k, \mathrm{y}_k, \mathrm{z}_k)^t$, respectively. The 1D detector (and hence the view plane) lies on the $\boldsymbol{Y}_k$–$\boldsymbol{Z}_k$ plane. An image with coordinates (u_k, v_k) is created by concatenating 1D images.

2 General Framework for Structure Recovery

In this section, we derive geometric constraints imposed by a pushbroom camera with 6 DOF motion. Then, we present equations for structure recovery and an epipolar curve based on the geometric constraints.

2.1 Imaging Geometry

Figure 2 depicts the imaging geometry of a pushbroom camera. The world coordinate system is denoted by $\boldsymbol{X}_{\mathrm{w}}$, $\boldsymbol{Y}_{\mathrm{w}}$ and $\boldsymbol{Z}_{\mathrm{w}}$. The camera captures a scene at discrete instants of time represented by kT_s, where k ($k = 0, 1, 2, \ldots$) is the time index and T_s is the sampling interval. The camera motion at the time instant kT_s is represented by the rotation matrix $\boldsymbol{R}_k$ and translation vector $\boldsymbol{t}_k$, which define the camera coordinate system given by $\boldsymbol{X}_k$, $\boldsymbol{Y}_k$ and $\boldsymbol{Z}_k$.

The 1D detector of the camera lies on the $\boldsymbol{Y}_k$–$\boldsymbol{Z}_k$ plane and it produces a 1D image at every time instant. By concatenating successive 1D images, we can produce an image with coordinates (u_k, v_k). The u coordinate represents the discrete time. That is:

$$u_k = kT_s \,. \tag{1}$$

The v coordinate represents spatial information. Consider a 3D scene point P whose camera coordinates are $\boldsymbol{p}_k = (\mathrm{x}_k, \mathrm{y}_k, \mathrm{z}_k)^t$. Its v coordinate is determined by a 1D perspective projection as:

$$v_k = \frac{f\mathrm{y}_k}{\mathrm{z}_k} + p_v \,, \tag{2}$$

where, f and p_v are the focal length and the image center, respectively.

2.2 Deriving Geometric Constraints

We denote the world coordinates of the 3D point P as $\boldsymbol{p}_w = (\mathrm{x_w}, \mathrm{y_w}, \mathrm{z_w})^t$. We know that the camera and world coordinates are related to each other as:

$$\boldsymbol{p}_k = \left(\boldsymbol{R}_k^t \mid -\boldsymbol{R}_k^t \boldsymbol{t}_k\right) \begin{pmatrix} \boldsymbol{p}_w \\ 1 \end{pmatrix} , \tag{3}$$

where,

$$\boldsymbol{R}_k^t = (\boldsymbol{i}_k, \boldsymbol{j}_k, \boldsymbol{k}_k)^t \;,\; \boldsymbol{t}_k = (t_{xk}, t_{yk}, t_{zk})^t \;. \tag{4}$$

The rows of the rotation matrix, $\boldsymbol{i}_k$, $\boldsymbol{j}_k$ and $\boldsymbol{k}_k$, define the directions of the axes of the camera coordinate system, $\boldsymbol{X}_k$, $\boldsymbol{Y}_k$ and $\boldsymbol{Z}_k$.

We can express the camera coordinate x_k by expanding Eq.(3) as follows:

$$\mathrm{x}_k = \boldsymbol{i}_k \cdot \boldsymbol{p}_w - \boldsymbol{i}_k \cdot \boldsymbol{t}_k \,. \tag{5}$$

Note that, since the view plane (1D detector) lies on the $\boldsymbol{Y}_k$–$\boldsymbol{Z}_k$ plane, we have $\mathrm{x}_k = 0$. Therefore, we have:

$$\boldsymbol{i}_k \cdot \boldsymbol{p}_w = \boldsymbol{i}_k \cdot \boldsymbol{t}_k \,. \tag{6}$$

The above expression which represents the view plane passing through the 3D point is called the *view plane equation*. It imposes a geometric constraint on the world coordinates $\boldsymbol{p}_w$ to recover scene structure.

Another constraint is obtained from the perspective projection of the 3D point to the 1D detector given by Eq.(2). Using y_k and z_k from Eq.(3), we have:

$$\boldsymbol{r}_k \cdot \boldsymbol{p}_w = \boldsymbol{r}_k \cdot \boldsymbol{t}_k \,, \tag{7}$$

$$\boldsymbol{r}_k = (v_k - p_v)\,\boldsymbol{k}_k - f\boldsymbol{j}_k \,. \tag{8}$$

In summary, we have two geometric constraints (Eqs. (6) and (7)) on the world coordinates of a scene point from one pushbroom camera.

2.3 Recovering Structure

We need three constraints to recover the three coordinates $\boldsymbol{p}_w = (\mathrm{x_w}, \mathrm{y_w}, \mathrm{z_w})^t$ of a scene point. As one camera yields only two constraints, we need one more camera. The view plane equations for the two cameras can be written as:

$$\boldsymbol{i}_{k1} \cdot \boldsymbol{p}_w = \boldsymbol{i}_{k1} \cdot \boldsymbol{t}_{k1} \;\text{ and }\; \boldsymbol{i}_{k2} \cdot \boldsymbol{p}_w = \boldsymbol{i}_{k2} \cdot \boldsymbol{t}_{k2} \,, \tag{9}$$

where, the time indices k_1 and k_2 represent the instants at which the cameras observe the 3D point.

The constraints obtained from the 1D projections are:

$$\boldsymbol{r}_{k1}\cdot\boldsymbol{p}_w = \boldsymbol{r}_{k1}\cdot\boldsymbol{t}_{k1} \text{ and } \boldsymbol{r}_{k2}\cdot\boldsymbol{p}_w = \boldsymbol{r}_{k2}\cdot\boldsymbol{t}_{k2}\,. \quad (10)$$

Using the above expressions, we can recover the coordinates of the 3D point, because we have four constraints and only three unknowns. For example, a matrix equation which has the following form can be constructed from Eq.(9) and the first expression in Eq.(10):

$$\boldsymbol{A}\boldsymbol{p}_w = \boldsymbol{b}\,, \quad (11)$$

$$\boldsymbol{A} = (\boldsymbol{i}_{k1}, \boldsymbol{i}_{k2}, \boldsymbol{r}_{k1},)^t\,, \quad (12)$$

$$\boldsymbol{b} = (\boldsymbol{i}_{k1}\cdot\boldsymbol{t}_{k1}, \boldsymbol{i}_{k2}\cdot\boldsymbol{t}_{k2}, \boldsymbol{r}_{k1}\cdot\boldsymbol{t}_{k1})^t\,. \quad (13)$$

The matrix $\boldsymbol{A}$ must satisfy Rank$\boldsymbol{A}$=3 to have a solution. When the camera motions are linear dependent then we have a degeneracy as Rank$\boldsymbol{A}$ <3 in that case.

We derive an explicit solution of structure by specifying the representation of the rotation, i.e., rotation angles around each axis of the camera coordinate system $(\theta_k, \phi_k, \psi_k)$, as shown in Appendix A. Using the rotation angles and the translation in Eq.(4), we denote camera motion by $(\theta_k, \phi_k, \psi_k, t_{xk}, t_{yk}, t_{zk})$ hereafter.

2.4 Deriving Epipolar Curve Equation

To compute the structure using Eq.(11), we have to find out the time indices k_1 and k_2 representing the instants at which the cameras observe the same 3D point. Since k_1 and k_2 are column numbers in stereo images (Eq.(1)), they can be determined by finding correspondences (feature matching) between two images. An epipolar constraint is used to find the correspondences. This constraint appears as an epipolar curve in an image, which can be represented by a function $v_{k2} = f\,(u_{k2}; u_{k1}, v_{k1})$, where (u_{k1}, v_{k1}) and (u_{k2}, v_{k2}) represent the coordinates in two images. A concrete expression of the function is obtained by backprojecting a view ray of the first camera into the image plane of the second camera. In stereo using pushbroom cameras, the backprojection of a view ray is equivalent to the following backprojection of a 3D point because a 1D detector is used:

$$v'_{k2} = v_{k2} - p_{v2} = \frac{f_2 \mathrm{y}_{k2}}{\mathrm{z}_{k2}}\,, \quad (14)$$

where, y_{k2} and z_{k2} are the camera coordinates computed from Eq.(3) as follows:

$$\mathrm{y}_{k2} = \boldsymbol{j}_{k2}\cdot\boldsymbol{p}_w - \boldsymbol{j}_{k2}\cdot\boldsymbol{t}_{k2}\,, \quad (15)$$

$$\mathrm{z}_{k2} = \boldsymbol{k}_{k2}\cdot\boldsymbol{p}_w - \boldsymbol{k}_{k2}\cdot\boldsymbol{t}_{k2}\,. \quad (16)$$

Since we have explicit expression of the structure $\boldsymbol{p}_w$, we can derive the explicit expression of the epipolar curve as shown in Appendix B.

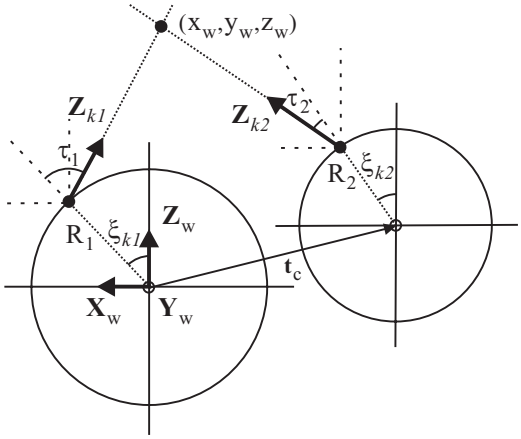

Figure 3: The camera configuration for polycentric panoramas [13]. Two cameras can have the different centers of rotation represented by the translation $\boldsymbol{t}_c = (t_{cx}, t_{cy}, t_{cz})^t$, radii, R_1 and R_2, and directions, τ_1 and τ_2.

The equations for structure recovery and the epipolar curve we derive are general in that it can be applied to 6 DOF camera motion. In the next section, we will demonstrate the generality of the results by analyzing a class of camera motion using the equations in Appendices A and B.

3 Special Cases: Vertical View Plane Class

We consider special cases with lower DOF camera motions, which are important to make a link between our framework and practical camera setup. This situation is quite similar to that of image-based rendering (IBR). In IBR, sampling of every light rays based on the original plenoptic function is very difficult because its dimension is 7 [22]. The methods using the plenoptic functions with lower dimensions, e.g., the light field [23] and concentric mosaic [24], were proposed to simplify camera motions to sample light rays. In our case, there are $\sum_{n=1}^{6} {}_6C_n = 63$ (n is DOF of motion) classes of camera motion. We select a class of camera motion with 5 DOF, i.e., $(\theta_k, \phi_k, 0, t_{xk}, t_{yk}, t_{zk})$, which we call *vertical view plane class* since the view plane of the camera with this motion is always vertical to the $\boldsymbol{X}$–$\boldsymbol{Z}$ plane of the world and camera coordinate systems due to elimination of the rotation around the $\boldsymbol{Z}$ axis. Especially we consider a subclass of the vertical view plane class with 4 DOF motion, $(0, \phi_k, 0, t_{xk}, t_{yk}, t_{zk})$, to show the relationship between our framework and previous results.

The equations for structure recovery and the epipolar curve of the subclass are obtained by just setting the rotation angles θ_{k1}, ψ_{k1}, θ_{k2} and ψ_{k2}

Table 1: Equations for the depth and epipolar curve of the camera configurations in the vertical view plane class with 4 DOF motion. In this table, $\Delta\phi_k = \phi_{k2} - \phi_{k1}$, $\Delta t_{xk} = t_{xk2} - t_{xk1}$, $\Delta t_{yk} = t_{yk2} - t_{yk1}$, $\Delta t_{zk} = t_{zk2} - t_{zk1}$, $v'_{k1} = v_{k1} - p_{v1}$ and $v'_{k2} = v_{k2} - p_{v2}$.

Camera configuration	depth	epipolar curve
Vertical view plane class (4 DOF)	$z_w = \{-\Delta t_{xk}\cos\phi_{k1}\cos\phi_{k2}$ $-t_{zk1}\sin\phi_{k1}\cos\phi_{k2}$ $+t_{zk2}\cos\phi_{k1}\sin\phi_{k2}\} / \sin(\Delta\phi_k)$	$v'_{k2} = \frac{f_2}{f_1} \cdot \frac{v'_{k1} T_{v2} + f_1 \Delta t_{yk} \sin(\Delta\phi_k)}{T_{v1}}$ $T_{v1} = \Delta t_{xk}\cos\phi_{k1} - \Delta t_{zk}\sin\phi_{k1}$ $T_{v2} = \Delta t_{xk}\cos\phi_{k2} - \Delta t_{zk}\sin\phi_{k2}$
Polycentric panoramas [13]	$z_w = (-R_1\cos\phi_{k2}\sin\tau_{k1} + R_2\cos\phi_{k1}\sin\tau_{k2}$ $-t_{cx}\cos\phi_{k1}\cos\phi_{k2}$ $+t_{cz}\cos\phi_{k1}\sin\phi_{k2}) / \sin(\Delta\phi_k)$	$v'_{k2} = \frac{f_2}{f_1} \cdot \frac{v'_{k1} T_{r2} + f_1 t_{cy} \sin(\Delta\phi_k)}{T_{r1}}$ $T_{r1} = R_1\sin\tau_{k1} + R_2\sin\delta_1 + t_{cx}\cos\phi_{k1}$ $-t_{cz}\sin\phi_{k1}$ $T_{r2} = R_1\sin\delta_2 - R_2\sin\tau_{k2} + t_{cx}\cos\phi_{k2}$ $-t_{cz}\sin\phi_{k2}$ $\delta_1 = \Delta\phi_k - \tau_{k2}$, $\delta_2 = \Delta\phi_k + \tau_{k1}$
Concentric mosaics [8, 9] [10, 11, 12]	$z_w = \frac{-R\sin\tau_{k1}}{\sin(\Delta\phi_k)/(\cos\phi_{k1}+\cos\phi_{k2})}$	$v'_{k2} = \frac{f_2}{f_1} \cdot v'_{k1}$
Parallel perspective [14, 15, 16, 21]	$z_w = \frac{\Delta t_{xk}}{2\tan\phi_{k1}} + \frac{t_{zk1}+t_{zk2}}{2}$	$v'_{k2} = \frac{f_2}{f_1} \cdot \frac{v'_{k1} T_{t2} - f_1 \Delta t_{yk} \sin(2\phi_{k1})}{T_{t1}}$ $T_{t1} = \Delta t_{xk}\cos\phi_{k1} - \Delta t_{zk}\sin\phi_{k1}$ $T_{t2} = \Delta t_{xk}\cos\phi_{k1} + \Delta t_{zk}\sin\phi_{k1}$

in Eqs.(22),(23),(24) and (35) to zero. We show the equations of the depth and epipolar curve in the first row of Tab.1.

We can directly apply the results to analyze previous work, e.g., polycentric panoramas [13]. Figure 3 shows the camera configuration for polycentric panoramas. Let the two cameras have the following motions: $(0, \phi_{k1}, 0, R_1\sin\xi_{k1}, 0, R_1\cos\xi_{k1})$ and $(0, \phi_{k2}, 0, t_{cx} + R_2\sin\xi_{k2}, t_{cy}, t_{cz} + R_2\cos\xi_{k2})$. The rotation angles of the camera coordinate systems ϕ_{k1} and ϕ_{k2} have the following relationship between the angles ξ_{k1} and ξ_{k2} which determine the position of the cameras and the angles τ_{k1} and τ_{k2}[1] which show the direction of the cameras with respect to the normal to the circle: $\phi_{k1} = \xi_{k1} + \tau_{k1}$ and $\phi_{k2} = \xi_{k2} + \tau_{k2}$. By substituting these camera motions into the equations of the vertical view plane class, we have the equations of the depth and epipolar curve for polycentric panoramas as shown in the second row of Tab.1.

For the case of stereo panoramas which have the same center of rotation and radii, and symmetric slits [8, 9, 10, 11, 12], i.e., $\boldsymbol{t}_c = \mathbf{0}$, $R_1 = R_2 = R$ and $\tau_{k1} = -\tau_{k2}$, we have the equations shown in the third row of Tab.1.

We also have the equations for parallel perspective stereo mosaic [14, 15, 16, 21] by just assuming the symmetric slits, i.e., $\phi_{k1} = -\phi_{k2}$. The result is shown in the fourth row of Tab.1.

Although our notations for camera motion are different from those used in the previous work, the equations shown in Tab.1 are equivalent to the depth and epipolar curve equations derived in the previous work. In summary, we demonstrate that several previous results are really special cases of our approach to stereo by multiperspective imaging.

4 Experimental Results

We show examples of the epipolar curves to verify the correctness of the equations derived in Appendices A and B. Figure 4 shows the epipolar curves for the images created by cameras with 6 and 5 DOF motions[2]. The small rectangles in the left images in the pairs show the feature points corresponding to the curves in the right images which pass through the matching points. These epipolar curves show the correctness of structure recovery because the epipolar curves which are the results of backprojection of the structure pass through

[1] In the rotation case, the angles τ_{k1} and τ_{k2} determine the position of slits in images used to create stereo images at the time k_1 and k_2 in the case where we use the camera with 2D CCD.

[2] We made the images using the 3D rendering software, POVRay [25].

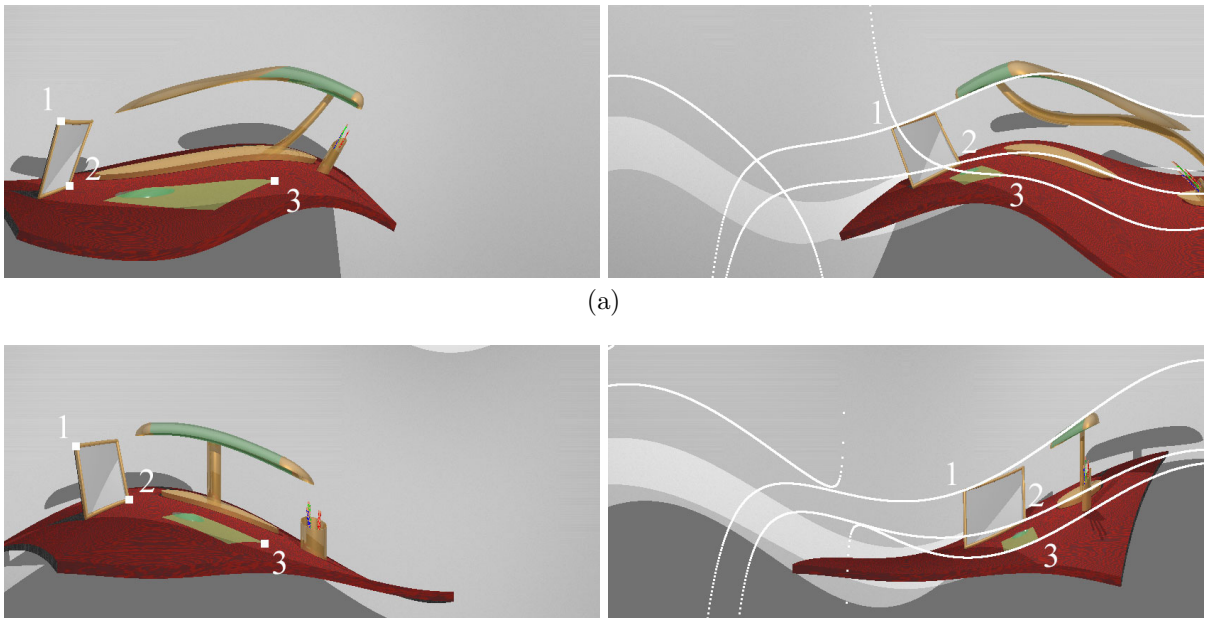

Figure 4: Epipolar curves for stereo images obtained from cameras with (a) 6 DOF $(\theta_k, \phi_k, \psi_k, t_{xk}, t_{yk}, t_{zk})$ and (b) 5 DOF $(\theta_k, \phi_k, 0, t_{xk}, t_{yk}, t_{zk})$ motions. The small rectangles in the left images in the pairs show the feature points corresponding to the curves in the right images which pass through the matching points. These results show that our results can be applied to general camera motion. Note that the distortion of the images are not uniform because the camera motions varied with time.

the correct matching points[3].

5 Summary

In this paper, we have presented a framework for stereo by multiperspective imaging. We derived the geometric constraints, the explicit representation of the equation for structure recovery and that for the epipolar curve for pushbroom cameras with 6 DOF motion. We showed that the several previous results for stereo panoramas can be viewed as special cases of our approach. The experiments were performed to show the correctness of the equations derived. We believe that the framework presented here will facilitate the design of stereo systems based on multiperspective imaging because it can be applied to arbitrary camera configurations.

A Equation for Structure Recovery

We use the following representation of the rotation matrix of Eq.(4) which shows the rotation around each axis of the camera coordinate system in Fig. 2:

$$\boldsymbol{R}_k^t = \boldsymbol{R}_x^t(\theta_k)\boldsymbol{R}_y^t(\phi_k)\boldsymbol{R}_z^t(\psi_k)\,, \tag{17}$$

[3]Some of the epipolar curves have singularity. A typical example is the curve corresponding to the feature "3" of the 5 DOF case. The singularity is produced by the solutions of Eq.(11) corresponding to "fake" structures in the back of cameras; the portion of the curves which do not pass through the correct matching point in Fig.4 are produced by the fake 3D structures.

where,

$$\boldsymbol{R}_x^t(\theta) = \begin{pmatrix} 1 & 0 & 0 \\ 0 & \cos\theta & \sin\theta \\ 0 & -\sin\theta & \cos\theta \end{pmatrix},$$

$$\boldsymbol{R}_y^t(\phi) = \begin{pmatrix} \cos\phi & 0 & -\sin\phi \\ 0 & 1 & 0 \\ \sin\phi & 0 & \cos\phi \end{pmatrix},$$

$$\boldsymbol{R}_z^t(\psi) = \begin{pmatrix} \cos\psi & \sin\psi & 0 \\ -\sin\psi & \cos\psi & 0 \\ 0 & 0 & 1 \end{pmatrix}.$$

The rows of the rotation matrix are given as follows:

$$\boldsymbol{i}_k = (\cos\phi_k\cos\psi_k, \cos\phi_k\sin\psi_k, -\sin\phi_k)^t\,, \tag{18}$$

$$\boldsymbol{j}_k = (-\cos\theta_k\sin\psi_k + \sin\theta_k\sin\phi_k\cos\psi_k, \cos\theta_k\cos\psi_k + \sin\theta_k\sin\phi_k\sin\psi_k, \sin\theta_k\cos\phi_k)^t\,, \tag{19}$$

$$\boldsymbol{k}_k = (\sin\theta_k\sin\psi_k + \cos\theta_k\sin\phi_k\cos\psi_k, -\sin\theta_k\cos\psi_k + \cos\theta_k\sin\phi_k\sin\psi_k, \cos\theta_k\cos\phi_k)^t \tag{20}$$

From Eq.(11), the structure $\boldsymbol{p}_w$ can be written as:

$$|\boldsymbol{A}|\,\boldsymbol{p}_w = \widetilde{\boldsymbol{A}}\boldsymbol{b}\,, \tag{21}$$

where, $\widetilde{\boldsymbol{A}}$ is the cofactor matrix of $\boldsymbol{A}$. Using the representation of the rotation matrix and the above equation, we have the following explicit representation of the equation for structure recovery from 6 DOF camera motion:

$$|\boldsymbol{A}|\,\mathrm{x_w} = s_{11} + s_{12} + s_{13}\,, \tag{22}$$

$$|\boldsymbol{A}|\,\mathrm{y_w} = s_{21} + s_{22} + s_{23}\,, \tag{23}$$

$$|\boldsymbol{A}|\,\mathrm{z_w} = s_{31} + s_{32} + s_{33}\,, \tag{24}$$

$$\begin{aligned}
|\boldsymbol{A}| &= -v_{k1}^{'}\sin\theta_{k1}\cos\phi_{k1}\sin\phi_{k2} \\
&-f_1\cos\theta_{k1}\cos\phi_{k1}\sin\phi_{k2} \\
&+v_{k1}^{'}\sin\theta_{k1}\sin\phi_{k1}\cos\phi_{k2}\cos\left(\Delta\psi_k\right) \\
&+f_1\cos\theta_{k1}\sin\phi_{k1}\cos\phi_{k2}\cos\left(\Delta\psi_k\right) \\
&+v_{k1}^{'}\cos\theta_{k1}\cos\phi_{k2}\sin\left(\Delta\psi_k\right) \\
&-f_1\sin\theta_{k1}\cos\phi_{k2}\sin\left(\Delta\psi_k\right),
\end{aligned} \tag{25}$$

$$\begin{aligned}
s_{11} &= -v_{k1}^{'}t_{xk1}\sin\theta_{k1}\cos\phi_{k1}\sin\phi_{k2} \\
&- f_1 t_{xk1}\cos\theta_{k1}\cos\phi_{k1}\sin\phi_{k2} \\
&+ v_{k1}^{'}t_{xk1}\cos\theta_{k1}\cos\phi_{k2}\cos\psi_{k1}\sin\psi_{k2} \\
&- f_1 t_{xk1}\sin\theta_{k1}\cos\phi_{k2}\cos\psi_{k1}\sin\psi_{k2} \\
&+ v_{k1}^{'}t_{xk1}\sin\theta_{k1}\sin\phi_{k1}\cos\phi_{k2}\sin\psi_{k1}\sin\psi_{k2} \\
&+ f_1 t_{xk1}\cos\theta_{k1}\sin\phi_{k1}\cos\phi_{k2}\sin\psi_{k1}\sin\psi_{k2} \\
&- v_{k1}^{'}t_{xk2}\cos\theta_{k1}\cos\phi_{k2}\sin\psi_{k1}\cos\psi_{k2} \\
&+ f_1 t_{xk2}\sin\theta_{k1}\cos\phi_{k2}\sin\psi_{k1}\cos\psi_{k2} \\
&+ v_{k1}^{'}t_{xk2}\sin\theta_{k1}\sin\phi_{k1}\cos\phi_{k2}\cos\psi_{k1}\cos\psi_{k2} \\
&+ f_1 t_{xk2}\cos\theta_{k1}\sin\phi_{k1}\cos\phi_{k2}\cos\psi_{k1}\cos\psi_{k2}\,,
\end{aligned} \tag{26}$$

$$\begin{aligned}
s_{12} &= -v_{k1}^{'}\Delta t_{yk}\cos\theta_{k1}\cos\phi_{k2}\sin\psi_{k1}\sin\psi_{k2} \\
&+ f_1\Delta t_{yk}\sin\theta_{k1}\cos\phi_{k2}\sin\psi_{k1}\sin\psi_{k2} \\
&+ v_{k1}^{'}\Delta t_{yk}\sin\theta_{k1}\sin\phi_{k1}\cos\phi_{k2}\cos\psi_{k1}\sin\psi_{k2} \\
&+ f_1\Delta t_{yk}\cos\theta_{k1}\sin\phi_{k1}\cos\phi_{k2}\cos\psi_{k1}\sin\psi_{k2}\,,
\end{aligned} \tag{27}$$

$$\begin{aligned}
s_{13} &= v_{k1}^{'}\Delta t_{zk}\cos\theta_{k1}\sin\phi_{k2}\sin\psi_{k1} \\
&- f_1\Delta t_{zk}\sin\theta_{k1}\sin\phi_{k2}\sin\psi_{k1} \\
&- v_{k1}^{'}\Delta t_{zk}\sin\theta_{k1}\sin\phi_{k1}\sin\phi_{k2}\cos\psi_{k1} \\
&- f_1\Delta t_{zk}\cos\theta_{k1}\sin\phi_{k1}\sin\phi_{k2}\cos\psi_{k1}\,,
\end{aligned} \tag{28}$$

$$\begin{aligned}
s_{21} &= v_{k1}^{'}\Delta t_{xk}\cos\theta_{k1}\cos\phi_{k2}\cos\psi_{k1}\cos\psi_{k2} \\
&- f_1\Delta t_{xk}\sin\theta_{k1}\cos\phi_{k2}\cos\psi_{k1}\cos\psi_{k2} \\
&+ v_{k1}^{'}\Delta t_{xk}\sin\theta_{k1}\sin\phi_{k1}\cos\phi_{k2}\sin\psi_{k1}\cos\psi_{k2} \\
&+ f_1\Delta t_{xk}\cos\theta_{k1}\sin\phi_{k1}\cos\phi_{k2}\sin\psi_{k1}\cos\psi_{k2}\,,
\end{aligned} \tag{29}$$

$$\begin{aligned}
s_{22} &= -v_{k1}^{'}t_{yk1}\cos\theta_{k1}\cos\phi_{k2}\sin\psi_{k1}\cos\psi_{k2} \\
&+ f_1 t_{yk1}\sin\theta_{k1}\cos\phi_{k2}\sin\psi_{k1}\cos\psi_{k2} \\
&- v_{k1}^{'}t_{yk1}\sin\theta_{k1}\cos\phi_{k1}\sin\phi_{k2} \\
&- f_1 t_{yk1}\cos\theta_{k1}\cos\phi_{k1}\sin\phi_{k2} \\
&+ v_{k1}^{'}t_{yk1}\sin\theta_{k1}\sin\phi_{k1}\cos\phi_{k2}\cos\psi_{k1}\cos\psi_{k2} \\
&+ f_1 t_{yk1}\cos\theta_{k1}\sin\phi_{k1}\cos\phi_{k2}\cos\psi_{k1}\cos\psi_{k2} \\
&+ v_{k1}^{'}t_{yk2}\cos\theta_{k1}\cos\phi_{k2}\cos\psi_{k1}\sin\psi_{k2} \\
&- f_1 t_{yk2}\sin\theta_{k1}\cos\phi_{k2}\cos\psi_{k1}\sin\psi_{k2} \\
&+ v_{k1}^{'}t_{yk2}\sin\theta_{k1}\sin\phi_{k1}\cos\phi_{k2}\sin\psi_{k1}\sin\psi_{k2} \\
&+ f_1 t_{yk2}\cos\theta_{k1}\sin\phi_{k1}\cos\phi_{k2}\sin\psi_{k1}\sin\psi_{k2}\,,
\end{aligned} \tag{30}$$

$$\begin{aligned}
s_{23} &= -v_{k1}^{'}\Delta t_{zk}\cos\theta_{k1}\sin\phi_{k2}\cos\psi_{k1} \\
&+ f_1\Delta t_{zk}\sin\theta_{k1}\sin\phi_{k2}\cos\psi_{k1} \\
&- v_{k1}^{'}\Delta t_{zk}\sin\theta_{k1}\sin\phi_{k1}\sin\phi_{k2}\sin\psi_{k1} \\
&- f_1\Delta t_{zk}\cos\theta_{k1}\sin\phi_{k1}\sin\phi_{k2}\sin\psi_{k1}\,,
\end{aligned} \tag{31}$$

$$\begin{aligned}
s_{31} &= v_{k1}^{'}\Delta t_{xk}\sin\theta_{k1}\cos\phi_{k1}\cos\phi_{k2}\cos\psi_{k2} \\
&+ f_1\Delta t_{xk}\cos\theta_{k1}\cos\phi_{k1}\cos\phi_{k2}\cos\psi_{k2}\,,
\end{aligned} \tag{32}$$

$$\begin{aligned}
s_{32} &= v_{k1}^{'}\Delta t_{yk}\sin\theta_{k1}\cos\phi_{k1}\cos\phi_{k2}\sin\psi_{k2} \\
&+ f_1\Delta t_{yk}\cos\theta_{k1}\cos\phi_{k1}\cos\phi_{k2}\sin\psi_{k2}\,,
\end{aligned} \tag{33}$$

$$\begin{aligned}
s_{33} &= v_{k1}^{'}t_{zk1}\sin\theta_{k1}\sin\phi_{k1}\cos\phi_{k2}\cos\left(\Delta\psi_k\right) \\
&+ f_1 t_{zk1}\cos\theta_{k1}\sin\phi_{k1}\cos\phi_{k2}\cos\left(\Delta\psi_k\right) \\
&+ v_{k1}^{'}t_{zk1}\cos\theta_{k1}\cos\phi_{k2}\cos\psi_{k1}\sin\psi_{k2} \\
&- f_1 t_{zk1}\sin\theta_{k1}\cos\phi_{k2}\cos\psi_{k1}\sin\psi_{k2} \\
&- v_{k1}^{'}t_{zk1}\cos\theta_{k1}\cos\phi_{k2}\sin\psi_{k1}\cos\psi_{k2} \\
&+ f_1 t_{zk1}\sin\theta_{k1}\cos\phi_{k2}\sin\psi_{k1}\cos\psi_{k2} \\
&- v_{k1}^{'}t_{zk2}\sin\theta_{k1}\cos\phi_{k1}\sin\phi_{k2} \\
&- f_1 t_{zk2}\cos\theta_{k1}\cos\phi_{k1}\sin\phi_{k2}\,.
\end{aligned} \tag{34}$$

where, $v_{k1}^{'} = v_{k1} - p_{v1}$, $\Delta\psi_k = \psi_{k2} - \psi_{k1}$, $\Delta t_{xk} = t_{xk2} - t_{xk1}$, $\Delta t_{yk} = t_{yk2} - t_{yk1}$ and $\Delta t_{zk} = t_{zk2} - t_{zk1}$.

B Equation for an Epipolar Curve

We can derive equation for the epipolar curve between two images captured by cameras with 6 DOF motions using the backprojection given by Eq.(14) and the structure given by the equations in Appendix A as follows:

$$v_{k2}^{'} = \frac{f_2\mathrm{y_{k2}}}{\mathrm{z_{k2}}} = \frac{f_2\cdot|\boldsymbol{A}|\,\mathrm{y_{k2}}}{|\boldsymbol{A}|\,\mathrm{z_{k2}}}\,, \tag{35}$$

$$|\boldsymbol{A}|\,\mathrm{y_{k2}} = e_{11} + e_{12} + e_{13}\,, \tag{36}$$

$$|\boldsymbol{A}|\,\mathrm{z_{k2}} = e_{21} + e_{22} + e_{23}\,, \tag{37}$$

$$\begin{aligned}
e_{11} &= v_{k1}^{'}\Delta t_{xk}\sin\theta_{k1}\sin\theta_{k2}\cos\phi_{k1}\cos\psi_{k2} \\
&+ f_1\Delta t_{xk}\cos\theta_{k1}\sin\theta_{k2}\cos\phi_{k1}\cos\psi_{k2} \\
&+ v_{k1}^{'}\Delta t_{xk}\cos\theta_{k1}\cos\theta_{k2}\cos\phi_{k2}\cos\psi_{k1} \\
&- f_1\Delta t_{xk}\sin\theta_{k1}\cos\theta_{k2}\cos\phi_{k2}\cos\psi_{k1} \\
&+ v_{k1}^{'}\Delta t_{xk}\sin\theta_{k1}\cos\theta_{k2}\sin\phi_{k1}\cos\phi_{k2}\sin\psi_{k1} \\
&+ f_1\Delta t_{xk}\cos\theta_{k1}\cos\theta_{k2}\sin\phi_{k1}\cos\phi_{k2}\sin\psi_{k1} \\
&- v_{k1}^{'}\Delta t_{xk}\sin\theta_{k1}\cos\theta_{k2}\cos\phi_{k1}\sin\phi_{k2}\sin\psi_{k2} \\
&- f_1\Delta t_{xk}\cos\theta_{k1}\cos\theta_{k2}\cos\phi_{k1}\sin\phi_{k2}\sin\psi_{k2}\,,
\end{aligned} \tag{38}$$

$$\begin{aligned}
e_{12} &= v_{k1}^{'}\Delta t_{yk}\cos\theta_{k1}\cos\theta_{k2}\cos\phi_{k2}\sin\psi_{k1} \\
&- f_1\Delta t_{yk}\sin\theta_{k1}\cos\theta_{k2}\cos\phi_{k2}\sin\psi_{k1} \\
&- v_{k1}^{'}\Delta t_{yk}\sin\theta_{k1}\cos\theta_{k2}\sin\phi_{k1}\cos\phi_{k2}\cos\psi_{k1} \\
&- f_1\Delta t_{yk}\cos\theta_{k1}\cos\theta_{k2}\sin\phi_{k1}\cos\phi_{k2}\cos\psi_{k1} \\
&+ v_{k1}^{'}\Delta t_{yk}\sin\theta_{k1}\cos\theta_{k2}\cos\phi_{k1}\sin\phi_{k2}\cos\psi_{k2} \\
&+ f_1\Delta t_{yk}\cos\theta_{k1}\cos\theta_{k2}\cos\phi_{k1}\sin\phi_{k2}\cos\psi_{k2} \\
&+ v_{k1}^{'}\Delta t_{yk}\sin\theta_{k1}\sin\theta_{k2}\cos\phi_{k1}\sin\psi_{k2} \\
&+ f_1\Delta t_{yk}\cos\theta_{k1}\sin\theta_{k2}\cos\phi_{k1}\sin\psi_{k2}\,,
\end{aligned} \tag{39}$$

$$\begin{aligned}
e_{13} &= v_{k1}^{'}\Delta t_{zk}\cos\theta_{k1}\sin\theta_{k2}\sin\psi_{k1}\cos\psi_{k2} \\
&- f_1\Delta t_{zk}\sin\theta_{k1}\sin\theta_{k2}\sin\psi_{k1}\cos\psi_{k2} \\
&- v_{k1}^{'}\Delta t_{zk}\sin\theta_{k1}\sin\theta_{k2}\sin\phi_{k1}\cos\psi_{k1}\cos\psi_{k2} \\
&- f_1\Delta t_{zk}\cos\theta_{k1}\sin\theta_{k2}\sin\phi_{k1}\cos\psi_{k1}\cos\psi_{k2} \\
&- v_{k1}^{'}\Delta t_{zk}\sin\theta_{k1}\sin\theta_{k2}\sin\phi_{k1}\sin\psi_{k1}\sin\psi_{k2} \\
&- f_1\Delta t_{zk}\cos\theta_{k1}\sin\theta_{k2}\sin\phi_{k1}\sin\psi_{k1}\sin\psi_{k2} \\
&- v_{k1}^{'}\Delta t_{zk}\cos\theta_{k1}\sin\theta_{k2}\cos\psi_{k1}\sin\psi_{k2} \\
&+ f_1\Delta t_{zk}\sin\theta_{k1}\sin\theta_{k2}\cos\psi_{k1}\sin\psi_{k2} \\
&- v_{k1}^{'}\Delta t_{zk}\cos\theta_{k1}\cos\theta_{k2}\sin\phi_{k2}\cos\left(\Delta\psi_k\right)
\end{aligned}$$

$$
\begin{aligned}
&+ f_1 \Delta t_{zk} \sin\theta_{k1} \cos\theta_{k2} \sin\phi_{k2} \cos(\Delta\psi_k) \\
&+ v'_{k1} \Delta t_{zk} \sin\theta_{k1} \cos\theta_{k2} \sin\phi_{k1} \sin\phi_{k2} \sin(\Delta\psi_k) \\
&+ f_1 \Delta t_{zk} \cos\theta_{k1} \cos\theta_{k2} \sin\phi_{k1} \sin\phi_{k2} \sin(\Delta\psi_k) , \quad (40) \\
e_{21} &= v'_{k1} \Delta t_{xk} \sin\theta_{k1} \cos\theta_{k2} \cos\phi_{k1} \cos\psi_{k2} \\
&+ f_1 \Delta t_{xk} \cos\theta_{k1} \cos\theta_{k2} \cos\phi_{k1} \cos\psi_{k2} \\
&+ v'_{k1} \Delta t_{xk} \sin\theta_{k1} \sin\theta_{k2} \cos\phi_{k1} \sin\phi_{k2} \sin\psi_{k2} \\
&+ f_1 \Delta t_{xk} \cos\theta_{k1} \sin\theta_{k2} \cos\phi_{k1} \sin\phi_{k2} \sin\psi_{k2} \\
&- v'_{k1} \Delta t_{xk} \cos\theta_{k1} \sin\theta_{k2} \cos\phi_{k2} \cos\psi_{k1} \\
&+ f_1 \Delta t_{xk} \sin\theta_{k1} \sin\theta_{k2} \cos\phi_{k2} \cos\psi_{k1} \\
&- v'_{k1} \Delta t_{xk} \sin\theta_{k1} \sin\theta_{k2} \sin\phi_{k1} \cos\phi_{k2} \sin\psi_{k1} \\
&- f_1 \Delta t_{xk} \cos\theta_{k1} \sin\theta_{k2} \sin\phi_{k1} \cos\phi_{k2} \sin\psi_{k1} , \quad (41) \\
e_{22} &= v'_{k1} \Delta t_{yk} \sin\theta_{k1} \cos\theta_{k2} \cos\phi_{k1} \sin\psi_{k2} \\
&+ f_1 \Delta t_{yk} \cos\theta_{k1} \cos\theta_{k2} \cos\phi_{k1} \sin\psi_{k2} \\
&- v'_{k1} \Delta t_{yk} \cos\theta_{k1} \sin\theta_{k2} \cos\phi_{k2} \sin\psi_{k1} \\
&+ f_1 \Delta t_{yk} \sin\theta_{k1} \sin\theta_{k2} \cos\phi_{k2} \sin\psi_{k1} \\
&- v'_{k1} \Delta t_{yk} \sin\theta_{k1} \sin\theta_{k2} \cos\phi_{k1} \sin\phi_{k2} \cos\psi_{k2} \\
&- f_1 \Delta t_{yk} \cos\theta_{k1} \sin\theta_{k2} \cos\phi_{k1} \sin\phi_{k2} \cos\psi_{k2} \\
&+ v'_{k1} \Delta t_{yk} \sin\theta_{k1} \sin\theta_{k2} \sin\phi_{k1} \cos\phi_{k2} \cos\psi_{k1} \\
&+ f_1 \Delta t_{yk} \cos\theta_{k1} \sin\theta_{k2} \sin\phi_{k1} \cos\phi_{k2} \cos\psi_{k1} , \quad (42) \\
e_{23} &= -v'_{k1} \Delta t_{zk} \sin\theta_{k1} \cos\theta_{k2} \sin\phi_{k1} \cos(\Delta\psi_k) \\
&- f_1 \Delta t_{zk} \cos\theta_{k1} \cos\theta_{k2} \sin\phi_{k1} \cos(\Delta\psi_k) \\
&- v'_{k1} \Delta t_{zk} \cos\theta_{k1} \cos\theta_{k2} \sin(\Delta\psi_k) \\
&+ f_1 \Delta t_{zk} \sin\theta_{k1} \cos\theta_{k2} \sin(\Delta\psi_k) \\
&+ v'_{k1} \Delta t_{zk} \cos\theta_{k1} \sin\theta_{k2} \sin\phi_{k2} \cos(\Delta\psi_k) \\
&- f_1 \Delta t_{zk} \sin\theta_{k1} \sin\theta_{k2} \sin\phi_{k2} \cos(\Delta\psi_k) \\
&- v'_{k1} \Delta t_{zk} \sin\theta_{k1} \sin\theta_{k2} \sin\phi_{k1} \sin\phi_{k2} \sin(\Delta\psi_k) \\
&- f_1 \Delta t_{zk} \cos\theta_{k1} \sin\theta_{k2} \sin\phi_{k1} \sin\phi_{k2} \sin(\Delta\psi_k) . \quad (43)
\end{aligned}
$$

References

[1] M. Irani and P. Anandan: "Video indexing based on mosaic representations," Proc. IEEE, Vol.86, pp.237-252, 1998

[2] D. Capel and A. Zisserman: "Automated mosaicing with super-resolution zoom," Proc. CVPR'98, pp.885-891, 1998

[3] M. Irani and P. Anandan: "About direct methods," Proc. Int. Workshop on Vision Algorithms, pp.267-277, 2000

[4] P. H. S. Torr and A. Zisserman: "Feature based methods for structure and motion estimation," Proc. Int. Workshop on Vision Algorithms, pp.278-294, 2000

[5] J. Zheng and S. Tsuji: "Panoramic representation for route recognition by a mobile robot," Int. J. Computer Vision, Vol.9, pp.55-76, 1992.

[6] S. Peleg and J. Herman: "Panoramic mosaics by manifold projection," Proc. CVPR'97, pp.338-343, 1997

[7] P. Rademacher and G. Bishop: "Multiple-center-of-projection images," Proc. SIGGRAPH'98, pp.199-206, 1998

[8] H. Ishiguro, H. Yamamoto and S. Tsuji: "Omni-directional Stereo," IEEE Trans. Pattern Anal. & Mach. Intell., Vol.14, pp.257-262, 1992

[9] S. Peleg and M. Ben-Ezra: "Stereo panoramas with a single camera," Proc. CVPR'99, pp.395-401, 1999

[10] H. Y. Shum and R. Szeliski: "Stereo reconstruction from multiperspective panoramas," Proc. ICCV'99, pp.14-21, 1999

[11] F. Huang: "Epipolar geometry in concentric panoramas," Research report of Czech Technical University, CTU-CMP-2000-07.

[12] P. Peer and F. Solina: "Panoramic depth imaging: single standard camera approach," Int. J. Computer Vision, Vol.47, No.1/2/3, pp.149-160, 2002

[13] F. Huang, S. K. Wei and R. Klette: "Geometrical fundamentals of polycentric panoramas," Proc. ICCV'01, pp.560-565, 2001 g

[14] R. Gupta and R. I. Hartley: "Linear pushbroom cameras," IEEE Trans. Pattern Anal. & Mach. Intell., Vol.19, No.9, pp.963-975, 1997

[15] J. X. Chai and H. Y. Shum: "Parallel projections for stereo reconstruction," Proc. CVPR'00, Vol.II, pp.493-500, 2000

[16] Z. Zhu, E. M. Riseman and A. R. Hanson: "Parallel-Perspective Stereo Mosaics," Proc. ICCV'01, Vol.I, pp.345-352, 2001

[17] D. Feldman, T. Pajdla and D. Weinshall: "On the epipolar geometry of the crossed-slits projection ," Proc. ICCV'03, pp.988-995, 2003

[18] A. Zomet, D. Feldman, S. Peleg and D. Weinshall: "Mosaicing new views: the crossed-slits projection," IEEE Trans. Pattern Anal. & Mach. Intell., Vol.25, No.6, pp.741-754, 2003

[19] J. Grodecki and D. Gene: "IKONOS geometric accuracy," Proc. Joint Workshop of ISPRS Working Groups I/2,I/5 and IV/7 on High Resolution Mapping from Space 2001.

[20] H. Y. Lee and W. Park: "A new epipolarity model based on the simplified pushbroom sensor model," Proc. Geospatial Theory, Processing and Applications, ISPRS Commission IV Symposium 2002.

[21] S. M. Seitz and J. Kim: "The space of all stereo images," Int. J. Computer Vision, Vol.48, No.1, pp.21-38, 2002

[22] E. H. Adelson and J. R. Bergen: "The plenoptic function and the elements of early vision," Computational Models of Visual Processing, pp.3-20, 1991

[23] M. Levoy and P. Hanrahan: "Light field rendering," Proc. SIGGRAPH'96, pp.31-42, 1996

[24] H. Y. Shum and L. W. He: "Rendering with concentric mosaics," Proc. SIGGRAPH'99, pp.299-306, 1999

[25] http://www.povray.org/